Brief Report

Structural Transitions at Microtubule Ends Correlate with Their Dynamic Properties in *Xenopus* Egg Extracts

Isabelle Arnal,*‡ **Eric Karsenti,*** **and Anthony A. Hyman**‡

*Cell Biology Program, European Laboratory of Molecular Biology, 69117 Heidelberg, Germany; and ‡Max Planck Institut for Molecular Cell Biology and Genetics, Dresden D-01307, Germany

Abstract. Microtubules are dynamically unstable polymers that interconvert stochastically between growing and shrinking states by the addition and loss of subunits from their ends. However, there is little experimental data on the relationship between microtubule end structure and the regulation of dynamic instability. To investigate this relationship, we have modulated dynamic instability in *Xenopus* egg extracts by adding a catastrophe-promoting factor, Op18/stathmin. Using electron cryomicroscopy, we find that microtubules in cytoplasmic extracts grow by the extension of a two-dimensional sheet of protofilaments, which later closes into a tube. Increasing the catastrophe frequency by the addition of Op18/stathmin decreases both the length and frequency of the occurrence of sheets and increases the number of frayed ends. Interestingly, we also find that more dynamic populations contain more blunt ends, suggesting that these are a metastable intermediate between shrinking and growing microtubules. Our results demonstrate for the first time that microtubule assembly in physiological conditions is a two-dimensional process, and they suggest that the two-dimensional sheets stabilize microtubules against catastrophes. We present a model in which the frequency of catastrophes is directly correlated with the structural state of microtubule ends.

Key words: microtubules • dynamic instability • *Xenopus* egg extracts • electron cryomicroscopy • protofilament sheets

Introduction

Microtubules are dynamic polymers that switch stochastically and infrequently between growing and shrinking states (Walker et al., 1988). This unusual behavior, called dynamic instability (Mitchison and Kirschner, 1984; Horio and Hotani, 1986), allows rapid spatial changes of the microtubule cytoskeleton during the cell cycle. A particularly striking example of such a rearrangement is the dramatic reorganization of microtubules during the interphase–mitosis transition (Hyman and Karsenti, 1996).

Many studies have been performed with pure tubulin to investigate the basic mechanism underlying dynamic instability. Microtubules elongate by the addition of tubulin dimers, which rapidly hydrolyze one of their two bound GTP molecules (Carlier, 1989). The energy coming from tubulin-GTP hydrolysis is essential to destabilize the microtubule lattice and allow its fast depolymerization (Hyman et al., 1992). For many years, the most popular model proposed that growing microtubules are stabilized by a terminal cap of unhydrolyzed GTP subunits (for review see Erickson and O'Brien, 1992), the loss of which would result in a sudden change between growing and shrinking states (termed a catastrophe). However, no GTP-tubulin has been detected at the present in the lattice of dynamic microtubules, and the GTP cap model remains controversial.

More recently, structural approaches using EM analysis of pure tubulin polymerization have shown that the regulation of both microtubule assembly and dynamics involves changes in their end structure. Two-dimensional sheets of tubulin are observed at the end of growing microtubules, whereas shrinking microtubules display curved protofilaments peeling out from their ends (Erickson, 1974; Kirschner et al., 1974, 1975; Simon and Salmon, 1990; Mandelkow et al., 1991; Chrétien et al., 1995; Tran et

al., 1997a; Müller-Reichert et al., 1998). Therefore, the conversion between growing and shrinking events involves a large structural change at the microtubule ends. One recent model to explain microtubule dynamics is based on the elastic properties of the polymer (Chrétien et al., 1995; Jánosi et al., 1998): a two-dimensional tubulin sheet at the end of the microtubule would act as a structural cap to stabilize it in a growing state. The complete closure of this sheet into a tube would induce shrinking events by promoting the release of intrinsically curved protofilaments (Kirschner et al., 1974; Howard and Timasheff, 1986; Melki et al., 1989; Mandelkow et al., 1991; Hyman et al., 1995; Tran et al., 1997a; Müller-Reichert et al., 1998). How the biochemical properties of tubulin contribute to this mechanism is still a matter of debate.

To understand the relationship between end structure and dynamics, it is important to look at a population of microtubules undergoing dynamic instability. In a population of microtubules growing in vitro, there are very few catastrophes, making it difficult to correlate growing and shrinking microtubules with their end structure (Chrétien et al., 1995). In vivo, microtubules are much more dynamic (Sammak and Borisy, 1988; Belmont et al., 1990; Simon et al., 1992), but to date no studies of microtubule end structure have been performed under physiological conditions.

To investigate the structural basis of dynamic instability under physiological conditions, we analyzed microtubule end structure and dynamics in *Xenopus* egg extracts. We find that physiological microtubule assembly occurs by the growth of two-dimensional sheets of tubulin, which later close into a tube. To correlate potential changes in end structures with dynamics, we increased the catastrophe frequency by adding the destabilizing factor Op18/stathmin (Belmont and Mitchison, 1996) to extracts. The results show that the increase in the catastrophe frequency induced by Op18/stathmin is accompanied by a decrease in both the length and proportion of the sheets and a concomitant increase in blunt and frayed ends. These results allow us to propose a structural model to explain dynamic instability and its possible relationship with GTP hydrolysis.

Materials and Methods

Purification of Recombinant Op18/Stathmin

Recombinant Op18/stathmin with a 6-histidine tag was purified from *Escherichia coli* as follows. 5 h after induction by 0.2 mM isopropyl-β-D-thiogalactopyranoside at 37°C, the cells were pelleted by centrifugation at 4°C and resuspended in buffer A (20 mM Tris and 100 mM NaCl, pH 6.8) supplemented with PMSF (1 mM) and protease inhibitor (leupeptin, pepstatin, and aprotinin, 100 μg/μl). The cells were lysed using the French Press, the extract was clarified at 17,000 rpm for 30 min at 4°C, and the supernatant was incubated with a metal affinity resin (Talon™ IMAC Resin; CLONTECH) for 1 h at 4°C. After washing the resin with buffer A and buffer A with 10 mM imidazole, the bound protein was eluted with 100 mM imidazole and dialyzed against BRB80 buffer (80 mM potassium-Pipes, 1 mM MgCl₂, and 1 mM EGTA, pH 6.8). Protein concentration was measured using a Bradford assay with BSA as a reference (calculated molecular mass of recombinant Op18/stathmin, 18,359 kD).

Preparation of Extracts

CSF *Xenopus* extracts (arrested in metaphase II of meiosis) were prepared as described before (Murray, 1991) and cycled into interphase by addition of 0.4 mM calcium and 200 μg/μl cycloheximide and incubation for 40 min at room temperature.

Video Microscopy and Data Analysis

Microtubule dynamics were measured in 10,000 *g* frog egg extracts supplemented with human purified centrosomes (2 × 10⁸ centrosomes/ml; Bornens et al., 1987), rhodamine tubulin (Hyman et al., 1991), saturated hemoglobin, and anti-Fade solution as described before (Tournebize et al., 1997). Dynamics were recorded using a Zeiss Axioskop, a 100× Apochromate lens (NA 1.4), and a rhodamine filter cube. Images were recorded every 4 s on an 8-bit black and white camera (Sony SSC-M370CE) with an image processor (model Argus 10; Hamamatsu) and stored on a Macintosh using NIH-Image software. Data analysis was done with a Microsoft Excel Macro to determine the growth rate, the shrinkage rate, and the catastrophe frequency of microtubules (Tournebize et al., 1997). For the experiments with Op18/stathmin, extracts supplemented with 3, 6, or 7.5 μM of the recombinant protein were similarly analyzed. Four experiments (0 μM Op18/stathmin) and two experiments (3, 6, and 7.5 μM Op18/stathmin), which were made in different extracts, were averaged. Differences between experiments with and without Op18/stathmin were evaluated using a *t* test with a confidence level of 95%. The percentage of time spent in the growing and shrinking states was determined by dividing the time recorded in growing (or shrinking) state by the total time recorded.

Specimen Preparation and Electron Cryomicroscopy

Vitreous ice–embedded samples were prepared as reported previously (Dubochet et al., 1985). 15 μl of interphasic extract were mixed on ice with 5 μl of purified human centrosomes (2 × 10⁸ centrosomes/ml). 2-μl samples were pipetted onto a holey carbon grid and incubated for 20 s in a humid atmosphere at 25–26°C (Chrétien et al., 1992). The droplet was blotted and plunged quickly into liquid ethane. For the experiments with Op18/stathmin, we followed the same procedure using interphasic extracts mixed on ice with centrosomes and different amounts of recombinant Op18/stathmin. The assembly time on the holey carbon grid was the same (20 s) except with 7.5 μM Op18/stathmin, for which the sample was incubated for 1 min (because of the shorter microtubules obtained in this case; see Results). Specimens were stored in liquid nitrogen and observed in a Philips CM 20 operating at 160 kV. Images were recorded under low dose conditions at a magnification of 27,500 and ∼2.5 μm underfocused.

Image Analysis

Micrographs were printed and microtubule end structures were analyzed directly on these prints. Three types of extremities were observed: (1) blunt ends (straight protofilaments or very short protofilament protrusions <30 nm); (2) extensions between 30 nm and 1.5 μm; and (3) spread-out ends (separated protofilaments). The percentage of each type of microtubule ends were calculated with respect to the total number of extremities that we could identify (235 with 0 μM Op18/stathmin, 84 with 3 μM Op18/stathmin, 63 with 6 μM Op18/stathmin, and 90 with 7.5 μM Op18/stathmin). A lot of extremities could not be classified because of the high background of granules and vesicles, which often hide tips of microtubules. Extension lengths were measured on the prints. We used the contrast present on microtubule images to localize the beginning of the extension, i.e., the point where the constant contrast and width of the complete cylinder is interrupted because of the apparition of one-sided curved extensions (Chrétien et al., 1995). The contrast of complete microtubules observed by electron cryomicroscopy was also used to determine the protofilament number (Chrétien and Wade, 1991).

Results

Two mechanisms have been proposed for the elongation of microtubules. One involves the helical addition of subunits to the tip of a growing microtubule (Chen and Hill, 1985; Bayley et al., 1990; Amos, 1995), whereas the other proposes the formation of two-dimensional protofilament sheets, which subsequently close into a tube (Erickson, 1974; Kirschner et al., 1975; Simon and Salmon, 1990; Chrétien et al., 1995). To determine the structural nature of microtubule ends elongating under physiological condi-
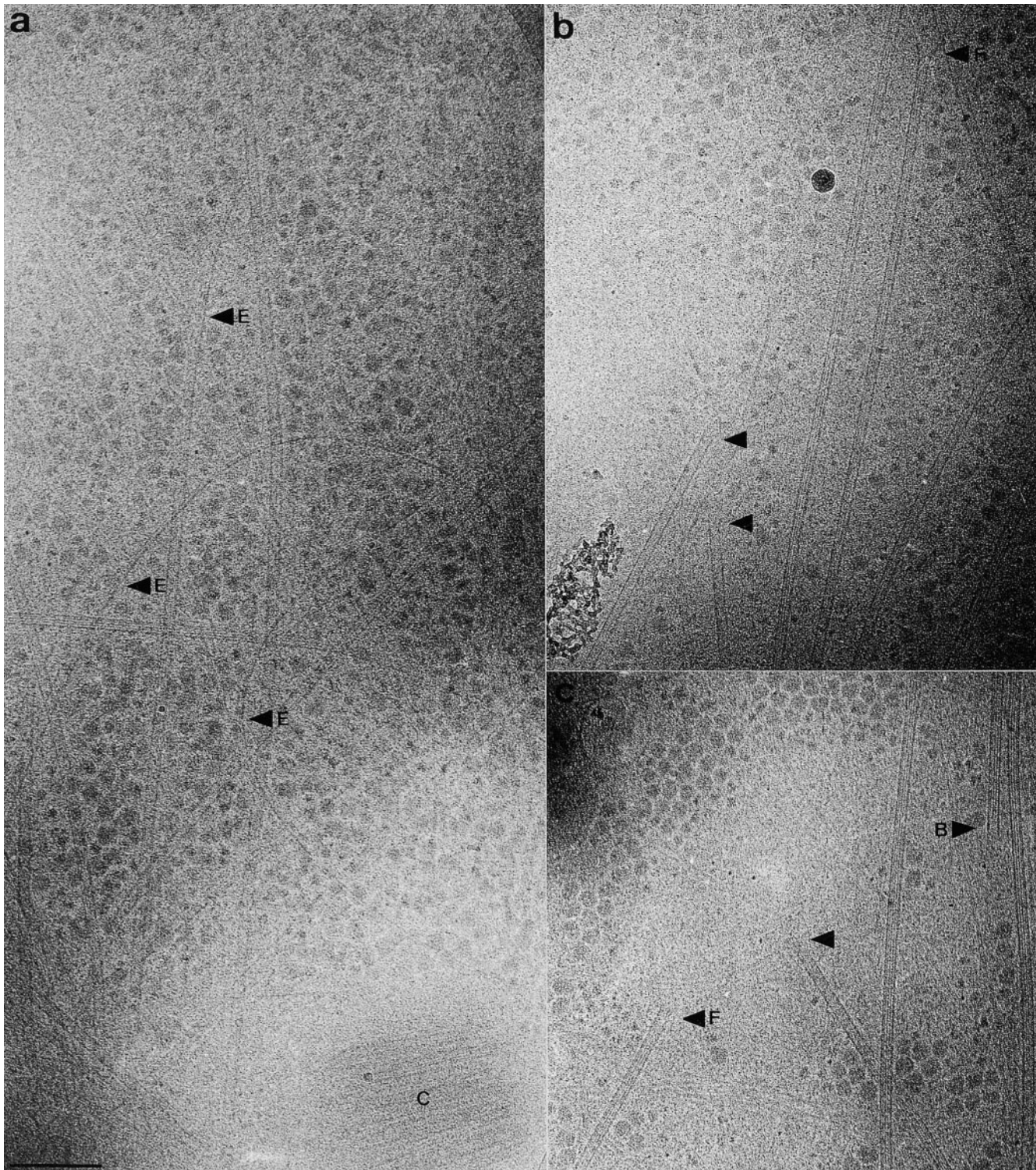
Figure 1. (a) Vitreous ice–embedded microtubules observed in interphasic extracts supplemented with isolated centrosomes and incubated for 20 s at 25°C. E, extensions observed at microtubule ends; and C, centriole. (b and c) Vitreous ice–embedded microtubules observed in interphasic extracts in the presence of 7.5 μM recombinant Op18/stathmin. Addition of Op18/stathmin in this condition induces the disappearance of sheets at microtubule ends (black arrows). F, frayed end; and B, blunt end. Bar, 200 nm.

tions, we examined microtubules nucleated off centrosomes in interphasic *Xenopus* egg extracts. Extracts supplemented with purified human centrosomes were frozen in liquid ethane after 20 s at room temperature, and the

frozen specimens were observed by electron cryomicroscopy. As shown in Fig. 1 a, the microtubules of the centrosomal aster are visible despite the high background from vesicles and granules present in these dense cytoplas-
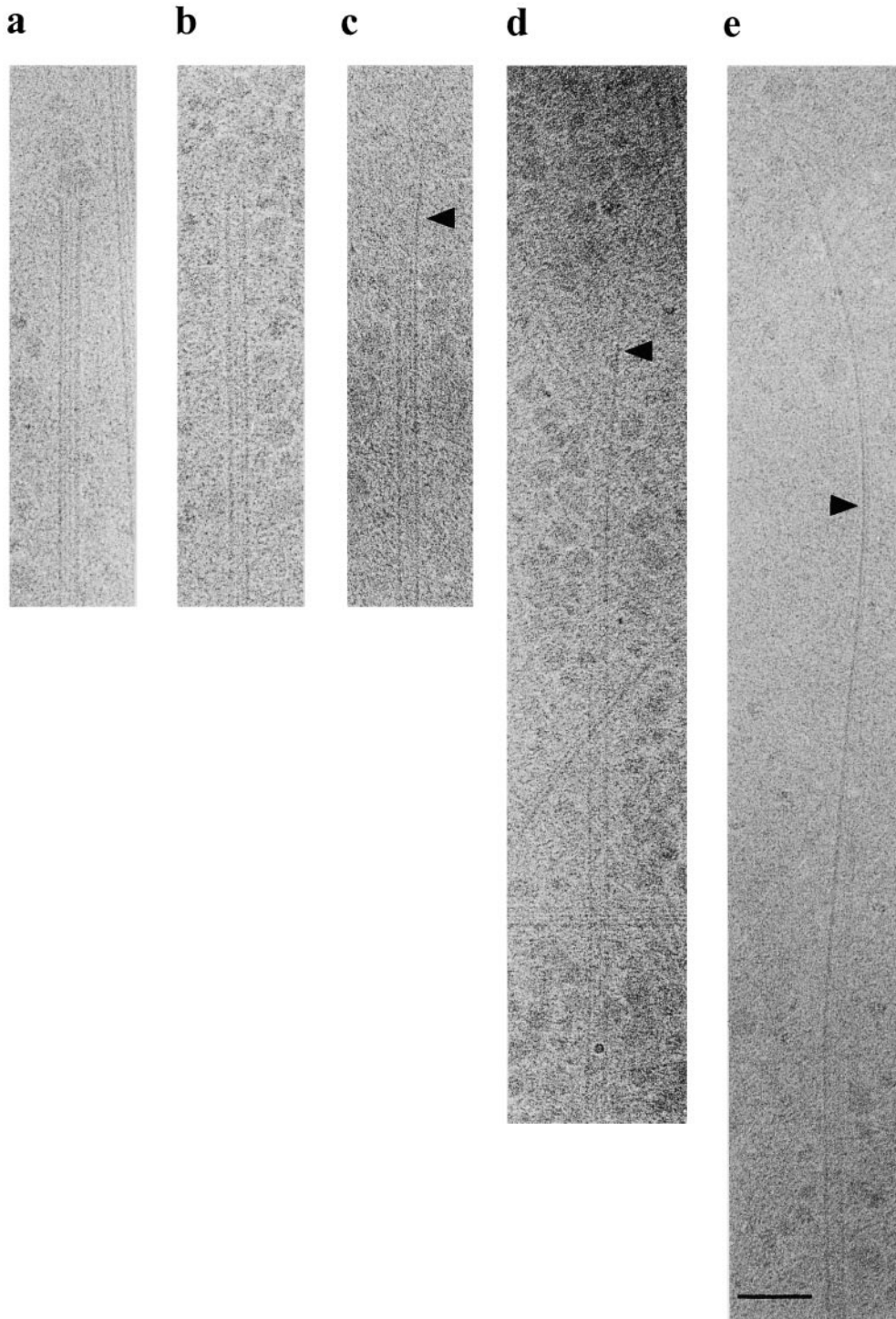
Figure 2. Detailed views of microtubule end structures in interphasic extracts. (a) Microtubule end with peeling protofilaments (frayed end). (b) Blunt end. (c–e) Extensions with variable lengths. Bar, 100 nm.

mic extracts. All microtubules observed have 13 protofilaments. Some of the microtubules show long extensions at their plus ends, which are easily recognized because they are curved and only one edge is visible, unlike the two parallel dark edges of the complete tube. These end structures are similar to those previously observed at the ends of microtubules assembled off centrosomes using pure tubulin and represent two-dimensional sheets of tubulin protofilaments (Chrétien et al., 1995).

Fig. 2 shows more detailed views of different end struc-

tures observed in extracts: microtubule extremities vary from blunt ends (Fig. 2 b) to extensions of variable lengths (Fig. 2, c–e). The average length is ∼440 nm with a distribution similar to the one described in vitro (Chrétien et al., 1995). Microtubules with frayed ends (split protofilaments) are also observed in interphasic extracts (Fig. 2 a). Microtubules with such end structures are most likely in a shrinking state (discussed further below; see Fig. 4). No microtubule ends were observed with tubulin oligomers, rings, or long curled protofilaments in extracts. These

a

Op18/stathmin 0 μM   Op18/stathmin 3 μM

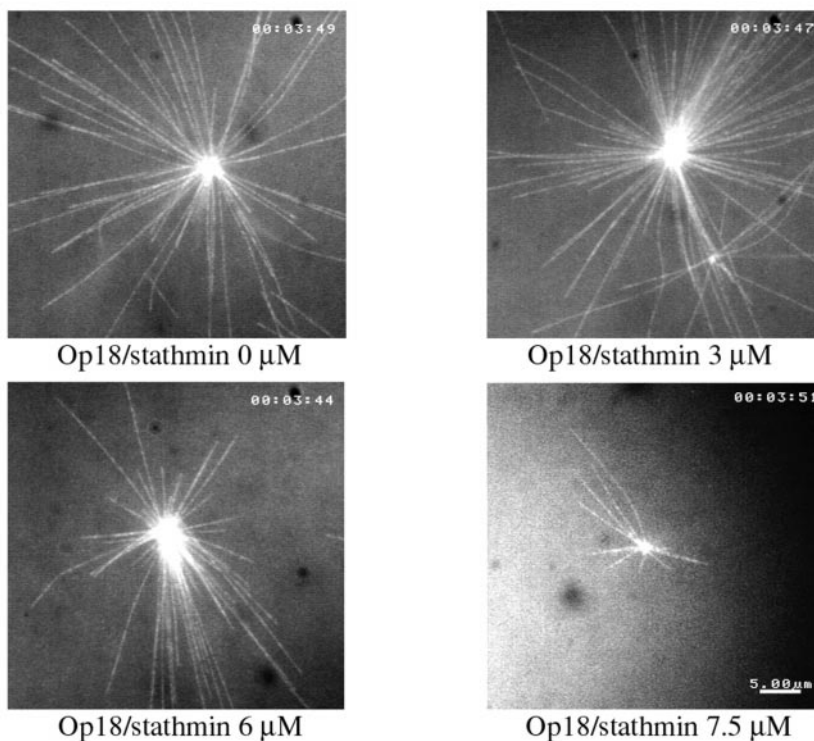Op18/stathmin 6 μM   Op18/stathmin 7.5 μM

b

Figure 3. (a) Op18/stathmin shortens microtubules in interphasic extracts. Images were taken from videos at the same time point after the beginning of the recording in the presence of 0, 3, 6, and 7.5 μM of recombinant Op18/stathmin added in interphasic extracts. (b) Op18/stathmin increases the catastrophe frequency in interphasic extract. The growth rate, shrinkage rate, and catastrophe frequency were determined from the movies recorded over time in interphasic extract with a different amount of Op18/stathmin. The rescue frequency is not reported because the number of events recorded was too low in most of the conditions.
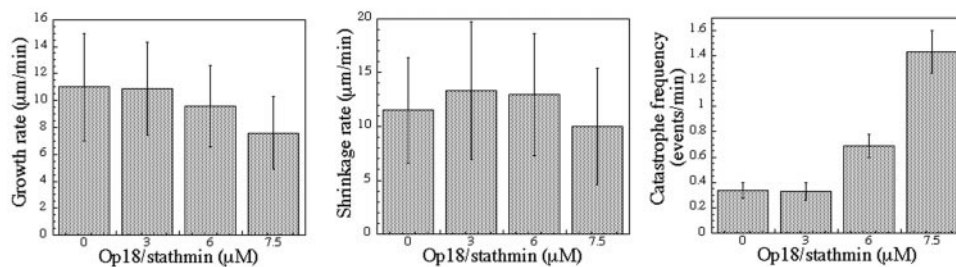
types of structures were mostly reported at the end of microtubules induced to shrink rapidly by a high calcium or magnesium concentrations or by cooling the sample (Kirschner et al., 1974; Simon and Salmon, 1990; Mandelkow et al., 1991; Tran et al., 1997a; Müller-Reichert et al., 1998).

These results establish that under physiological conditions, microtubules grow by elongation of a two-dimensional sheet that closes into a tube as previously proposed on the basis of experiments performed with pure tubulin (Erickson, 1974; Kirschner et al., 1975; Simon and Salmon, 1990; Chrétien et al., 1995).

To analyze the relationship between the structure of a microtubule end and its dynamic nature, we manipulated microtubule dynamics and assessed the consequences on end structure. *Xenopus* extracts are an excellent system to pursue such an investigation because the growing rate and catastrophe frequency can be independently manipulated by the exogenous addition of regulatory factors. To vary the catastrophe frequency, we added Op18/stathmin, which increases the catastrophe frequency of pure microtubules

(Belmont and Mitchison, 1996). The addition of Op18/stathmin reduces the average length of microtubules nucleated off centrosomes in interphase extracts in a dose-dependent manner (Fig. 3 a). Specifically, the addition of 3 μM Op18/stathmin does not change any of the dynamic properties of microtubules (Fig. 3 b, Table I). In contrast,

Table I. Addition of Recombinant Op18 in Interphasic Extracts Increases the Catastrophe Frequency

	Growth rate	Shrinkage rate	Catastrophe frequency
	μm/min	*μm/min*	*events/min*
Stathmin 0 μM	11 ± 4 (95)	11.51 ± 4.9 (29)	0.34 ± 0.05 (34)
Stathmin 3 μM	10.87 ± 3.44 (48)	13.3 ± 6.4 (19)	0.33 ± 0.07 (20)
Stathmin 6 μM	9.57 ± 3 (57)	12.94 ± 5.68 (38)	0.69 ± 0.09 (48)
Stathmin 7.5 μM	7.57 ± 2.7 (59)	10.0 ± 5.4 (49)	1.43 ± 0.17 (66)

Values represent the mean value ± SD of the mean (number of microtubules for the growth and shrinkage rate, number of events for the catastrophe frequency). The rescue frequency is not reported because the number of events recorded was too low in most of the conditions.
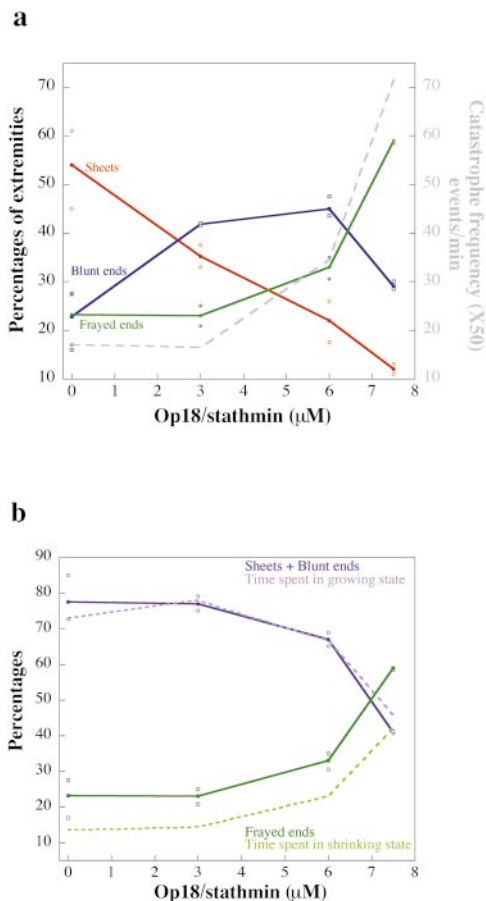
a

b

Figure 4. (a) Microtubule end structure in the presence of a different amount of recombinant Op18/stathmin added in interphasic extracts. Microtubule ends are represented as the percentage of the total number of extremities. Values are the mean of four (control) or two (3, 6, and 7.5 μM Op18/stathmin) experiments made in different extracts. For each condition, the mean value is represented by a closed symbol and the minimum and the maximum values by open symbols. (b) Microtubule end structure of growing and shrinking microtubules. The percentage of time spent in the growing state (light violet curve) as well as the combined proportion of sheets and blunt ends (dark violet curve) decrease with increased amount of recombinant Op18/stathmin added in interphasic extracts caused by the higher level of catastrophes. The percentage of time spent in the shrinking state (dark green curve) and the frayed end proportion (light green curve) follow the inverse change versus the Op18/stathmin concentration.

: GTP-Tubulin

Figure 5. Structural model explaining dynamic instability and its possible relationship with the GTP cap model. (a) Microtubules with two-dimensional sheets at their end are in a stable growing state. GTP-tubulin (in green) contained in the sheet could explain part of its stabilization capacity. When the tube closes, a few subunits in a GTP state at the extremity would be sufficient to maintain the microtubule in a growing state. (b) As soon as the GTP is hydrolyzed (c), the microtubule will explode because of the weak lateral interaction between GDP-tubulin (d). Blunt ends (b and c) are unstable because the loss of the GTP-tubulin subunits triggers them in a shrinking state, whereas sheets are always stable.

diate concentrations of Op18/stathmin (3 and 6 μM) and decreases as more microtubules exhibit frayed ends. The average length of sheets decreases from 440 nm without Op18/stathmin to 283 nm with 3 μM Op18/stathmin and varies between 120 and 208 nm at higher concentrations (these last values are only an estimate given the very low numbers of sheets observed with 6 and 7.5 μM Op18/stathmin, Fig. 4 a).

Next, we correlated the changes in the microtubule end structure with changes in the dynamic properties of microtubules after addition of Op18/stathmin (Fig. 4 b). In the absence of added Op18/stathmin, 73% of the microtubules are in a growing state (Fig. 4 b), but only 54% of them display sheets at their extremity (Fig. 4 a). These values suggest that not all growing microtubules have sheets at their ends. However, the combined percentage of sheets and blunt ends correlates precisely with the percentage of growing microtubules at different Op18/stathmin concentrations (Fig. 4 b, violet curves), suggesting that blunt ends also correspond to the growing microtubules. This suggestion is considerably strengthened by the strong correlation between the percentage of frayed ends and that of shrinking microtubules (Fig. 4 b, green curves). These results lead us to conclude that in *Xenopus* egg extracts, microtubules with protofilament sheets or blunt ends are in the growing state, whereas those with frayed ends are in the shrinking state.

One interesting observation we made is that the increase in catastrophe frequency is associated with an increase in the blunt end proportion (6 μM Op18/stathmin; Fig. 4 a) followed by a strong increase in the frayed end proportion (7.5 μM Op18/stathmin; Fig. 4 a). This result suggests that blunt ends are more unstable compared with the ends with sheets at their extremities. Blunt ends could either grow or transit to shrinkage with a certain probabil-

the addition of 6 μM Op18/stathmin and 7.5 μM Op18/stathmin increases the catastrophe rate twofold and fourfold, respectively. The shrinkage rate is not significantly different from unperturbed extracts at either 6 or 7.5 μM Op18/stathmin, whereas the growth rate is slightly decreased for the highest concentration used. We analyzed microtubule end structure by electron cryomicroscopy in the presence of 0, 3, 6, and 7.5 μM Op18/stathmin (Figs. 1 b and 4 a). Increasing the Op18/stathmin concentration reduces the proportion of sheets and increases the proportion of blunt and frayed microtubule ends (Fig. 4 a). The proportion of blunt ends increases transiently for interme-
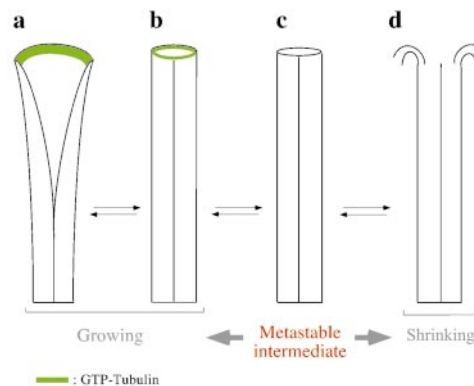
ity, whereas all microtubules with visible sheets at their ends are in a stable growing state. In apparent contradiction with this idea, at 3 µM Op18/stathmin, the proportion of blunt ends is greater than at 0 µM, but there is no significant increase in the catastrophe frequency. One possibility is that the probability of blunt ends to transit to the shrinking state is different at 3 and 6 µM Op18/stathmin despite their similar proportion. This is reflected in the greater number of frayed ends at 6 µM Op18/stathmin. Another possibility is that we may have classified as blunt ends some very short sheets made of a few protofilaments (as Op18/stathmin decreases the sheet length). In this case, a structural transition would occur between 3 and 6 µM Op18/stathmin, allowing the complete closure of the tube and increasing the probability of a shrinking event.

Discussion

Our results show that under physiological conditions, all microtubules with visible sheets at their ends are in the growing state and all microtubules with frayed ends are in the shrinking state. These observations conclusively demonstrate that physiological microtubule assembly occurs by the extension of two-dimensional protofilament sheets at microtubule ends and not by helical polymerization. The structure of depolymerizing ends observed in extracts suggests that under normal conditions of dynamic instability, microtubules shrink by loss of protofilaments that peel away from the tube and dissolve almost immediately into subunits. It seems likely that the rams horns, which are seen after microtubules are forced into shrinking by calcium or magnesium, are caused by stabilization of these structures by the agents used to trigger shrinking (Tran et al., 1997a). Less certain is the dynamic nature of microtubules with blunt ends. A possibility that we favor is that blunt ends represent a structural state that is a metastable intermediate between the growing and shrinking states (Tran et al., 1997b). Thus, microtubules with blunt ends may either grow or transit to shrinking with a certain probability. A similar metastable state has been postulated on the basis of kinetic studies of severed MT ends (Tran et al., 1997b).

One interesting question that arises from this study concerns the mechanism by which Op18/stathmin induces the disappearance of tubulin sheets at the end of growing microtubules and why the elimination of the sheets tends to result in an increase in the catastrophe frequency (as suggested in Fig. 4 a). Op18/stathmin could either prevent the elongation of sheets or increase the rate of tube closure. Each model has different predictions concerning the molecular mechanisms involved. The first model would imply that the addition of tubulin subunits at microtubule ends is slowed down by the presence of Op18/stathmin because of the sequestering of free tubulin dimers (Howell et al., 1999). The second model would predict that Op18/stathmin binds to the protofilaments and favors the curvature leading to tube formation over the outward curvature of the sheet (for review see Chrétien et al., 1999). Because Op18/stathmin does not significantly affect the rate of microtubule elongation under conditions in which catastrophe increases (specifically at 6 µM Op18/stathmin), and because of the evidence suggesting that it can act directly

at microtubule ends (Howell et al., 1999; Larsson et al., 1999), we favor the second model. However, the tubulin-sequestering activity of Op18/stathmin could also contribute to the increase in the catastrophe frequency at a higher concentration (7.5 µM) since we observed a slight decrease in the growth rate in this condition.

Why should the elimination of sheets make microtubules more prone to undergo a catastrophe? The tubulin dimer has an intrinsic curvature that causes tubulin protofilaments to have an outward curvature (Howard and Timasheff, 1986; Melki et al., 1989; Mandelkow et al., 1991; Hyman et al., 1995; Tran et al., 1997a; Müller-Reichert et al., 1998). When 13 protofilaments associate laterally and close into a tube, their outward curvature puts the microtubule wall under tension. Sheets at the end of a microtubule, therefore, make microtubules stable because they introduce a cap of relaxed interactions between protofilaments at the end of the mechanically strained tube polymer (Chrétien et al., 1995, 1999). Loss of the sheet as a consequence of tube closure catching up with sheet extension generates a blunt end that may either transit to shrinking or continue growing. What may influence the probability with which a blunt end transits to a shrinking phase? It seems likely to be associated with GTP-tubulin hydrolysis (Fig. 5). Only a few GTP-tubulin subunits are required to stabilize the ends of microtubules (Drechsel and Kirschner, 1994; Caplow and Shanks, 1996). We speculate that when a blunt end is generated by tube closure catching up with the sheet extension, the chemical composition of tubulin subunits at the blunt end will influence whether the end will transit to shrinking or continue growing. If GTP-tubulin subunits are at the blunt end, then the microtubule is more likely to grow. In contrast, if GDP-tubulin subunits are present, then the microtubule is more likely to transit to the shrinking state. Interestingly, it was suggested that Op18/stathmin triggers catastrophes by stimulating GTP hydrolysis (Larsson et al., 1999; Howell et al., 1999). This could also increase the probability of a blunt end to transit to the shrinking state in our model (Fig. 5). Nevertheless, such a mechanism does not explain the structural changes observed at the end of microtubules in the presence of Op18/stathmin, i.e., the disappearance of two-dimensional tubulin sheets. A definitive resolution of this issue will require the development of techniques capable of directly assessing the chemical nature of tubulin subunits in the end structures observed by cryo-EM.

References

Amos, L. 1995. The microtubule lattice: 20 years on. *Trends Cell Biol.* 5:48–51.
Bayley, P.M., M.J. Schilstra, and S.R. Martin. 1990. Microtubule dynamic instability: numerical simulation of microtubule transition properties using a lateral cap model. *J. Cell Sci.* 95:33–48.

Belmont, L.D., and T.J. Mitchison. 1996. Identification of a protein that interacts with tubulin dimers and increases the catastrophe rate of microtubules. *Cell.* 84:623–631.

Belmont, L.D., A.A. Hyman, K.E. Sawin, and T.J. Mitchison. 1990. Real-time visualization of cell cycle-dependent changes in microtubule dynamics in cytoplasmic extracts. *Cell.* 62:579–589.

Bornens, M., M. Paintrand, J. Berges, M.C. Marty, and E. Karsenti. 1987. Structural and chemical characterization of isolated centrosomes. *Cell Motil. Cytoskeleton.* 8:238–249.

Caplow, M., and J. Shanks. 1996. Evidence that a single monolayer tubulin-GTP cap is both necessary and sufficient to stabilize microtubules. *Mol. Biol. Cell.* 7:663–675.

Carlier, M.F. 1989. Role of nucleotide hydrolysis in the dynamics of actin filaments and microtubules. *Int. Rev. Cytol.* 115:139–170.

Chen, Y., and T.L. Hill. 1985. Monte Carlo study of the GTP cap in a five-start helix model of a microtubule. *Proc. Natl. Acad. Sci. USA.* 82:1131–1135.

Chrétien, D., and R.H. Wade. 1991. New data on the microtubule surface lattice. *Biol. Cell.* 71:161–174.

Chrétien, D., F. Metoz, F. Verde, E. Karsenti, and R.H. Wade. 1992. Lattice defects in microtubules: protofilament numbers vary within individual microtubules. *J. Cell Biol.* 117:1031–1040.

Chrétien, D., S.D. Fuller, and E. Karsenti. 1995. Structure of growing microtubule ends: two-dimensional sheets close into tubes at variable rates. *J. Cell Biol.* 129:1311–1328.

Chrétien, D., I. Jánosi, J.C. Taveau, and H. Flyvberg. 1999. Microtubule's conformational cap. *Cell Struct. Funct.* 24:299–303.

Drechsel, D.N., and M.W. Kirschner. 1994. The minimum GTP cap required to stabilize microtubules. *Curr. Biol.* 4:1053–1061.

Dubochet, J., M. Adrian, J. Lepault, and A.W. McDowall. 1985. Cryo-electron microscopy of vitrified biological specimens. *Trends Biochem. Soc.* 10:143–146.

Erickson, H.P. 1974. Microtubule surface lattice and subunit structure and observations on reassembly. *J. Cell Biol.* 60:153–167.

Erickson, H.P., and E.T. O'Brien. 1992. Microtubule dynamic instability and GTP hydrolysis. *Annu. Rev. Biophys. Biomol. Struct.* 21:145–166.

Horio, T., and H. Hotani. 1986. Visualization of the dynamic instability of individual microtubules by dark-field microscopy. *Nature.* 321:605–607.

Howard, W.D., and S.N. Timasheff. 1986. GDP state of tubulin: stabilization of double rings. *Biochemistry.* 25:8292–8300.

Howell, B., N. Larsson, M. Gullberg, and L. Cassimeris. 1999. Dissociation of the tubulin-sequestering and microtubule catastrophe-promoting activities of oncoprotein 18/stathmin. *Mol. Biol. Cell.* 10:105–118.

Hyman, A.A., and E. Karsenti. 1996. Morphogenetic properties of microtubules and mitotic spindle assembly. *Cell.* 84:401–410.

Hyman, A., D. Drechsel, D. Kellogg, S. Salser, K. Sawin, P. Steffen, L. Wordeman, and T. Mitchison. 1991. Preparation of modified tubulins. *Methods Enzymol.* 196:478–485.

Hyman, A.A., S. Salser, D.N. Drechsel, N. Unwin, and T.J. Mitchison. 1992. Role of GTP hydrolysis in microtubule dynamics: information from a slowly hydrolyzable analogue, GMPCPP. *Mol. Biol. Cell.* 3:1155–1167.

Hyman, A.A., D. Chrétien, I. Arnal, and R.H. Wade. 1995. Structural changes accompanying GTP hydrolysis in microtubules: information from a slowly hydrolyzable analogue guanylyl-(α,β)-methylene-diphosphonate. *J. Cell Biol.* 128:117–125.

Jánosi, I.M., D. Chrétien, and H. Flyvbjerg. 1998. Modeling elastic properties of microtubule tips and walls. *Eur. Biophys. J.* 27:501–513.

Kirschner, M.W., R.C. Williams, M. Weingarten, and J.C. Gerhart. 1974. Microtubules from mammalian brain: some properties of their depolymerization products and a proposed mechanism of assembly and disassembly. *Proc. Natl. Acad. Sci. USA.* 71:1159–1163.

Kirschner, M.W., L.S. Honig, and R.C. Williams. 1975. Quantitative electron microscopy of microtubule assembly in vitro. *J. Mol. Biol.* 99:263–276.

Larsson, N., B. Segerman, B. Howell, K. Fridell, L. Cassimeris, and M. Gullberg. 1999. Op18/stathmin mediates multiple region-specific tubulin and microtubule-regulating activities. *J. Cell Biol.* 146:1289–1302.

Mandelkow, E.M., E. Mandelkow, and R.A. Milligan. 1991. Microtubule dynamics and microtubule caps: a time-resolved cryo-electron microscopy study. *J. Cell Biol.* 114:977–991.

Melki, R., M.F. Carlier, D. Pantaloni, and S.N. Timasheff. 1989. Cold depolymerisation of microtubule to double rings: geometric stabilization of assemblies. *Biochemistry.* 28:9143–9152.

Mitchison, T., and M. Kirschner. 1984. Dynamic instability of microtubule growth. *Nature.* 312:237–242.

Müller-Reichert, T., D. Chrétien, F. Severin, and A.A. Hyman. 1998. Structural changes at microtubule ends accompanying GTP hydrolysis: information from a slowly hydrolyzable analogue of GTP, guanylyl(alpha,beta)methylenediphosphonate. *Proc. Natl. Acad. Sci. USA.* 95:3661–3666.

Murray, A.W. 1991. Cell cycle extracts. *In* Cell Cycle Extracts. B.K. Kay and H.B. Peng, editors. Academic Press Inc., San Diego. 581–605.

Sammak, P.J., and G.G. Borisy. 1988. Direct observation of microtubule dynamics in living cells. *Nature.* 332:724–726.

Simon, J.R., and E.D. Salmon. 1990. The structure of microtubule ends during the elongation and shortening phases of dynamic instability examined by negative-stain electron microscopy. *Cell Sci.* 96:571–582.

Simon, J.R., S.F. Parsons, and E.D. Salmon. 1992. Buffer conditions and nontubulin factors critically affect the microtubule dynamic instability of sea urchin egg tubulin. *Cell Motil. Cytoskeleton.* 21:1–14.

Tournebize, R., S.S. Andersen, F. Verde, M. Doree, E. Karsenti, and A.A. Hyman. 1997. Distinct roles of PP1 and PP2A-like phosphatases in control of microtubule dynamics during mitosis. *EMBO (Eur. Mol. Biol. Organ.) J.* 16:5537–5549.

Tran, P.T., P. Joshi, and E.D. Salmon. 1997a. How tubulin subunits are lost from the shortening ends of microtubules. *J. Struct. Biol.* 118:107–118.

Tran, P.T., R.A. Walker, and E.D. Salmon. 1997b. A metastable intermediate state of microtubule dynamic instability that differs significantly between plus and minus ends. *J. Cell Biol.* 138:105–117.

Walker, R.A., E.T. O'Brien, N.K. Pryer, M.F. Soboeiro, W.A. Voter, H.P. Erickson, and E.D. Salmon. 1988. Dynamic instability of individual microtubules analyzed by video light microscopy: rate constants and transition frequencies. *J. Cell Biol.* 107:1437–1448.